IEEE Access
Multidisciplinary | Rapid Review | Open Access Journal

Received September 12, 2019, accepted October 11, 2019, date of publication October 16, 2019, date of current version November 1, 2019.

Digital Object Identifier 10.1109/ACCESS.2019.2947415

Robust Energy Management in Active Distribution Systems Considering Temporal and Spatial Correlation

SUYANG ZHOU[1], YI ZHAO[1], WEI GU[1], (Senior Member, IEEE), ZHI WU[1,2], (Member, IEEE), YUNPENG LI[3], ZHONGHAO QIAN[3], AND YU JI[3]

[1]School of Electrical Engineering, Southeast University, Nanjing 210096, China
[2]Jangsu Key Laboratory of Smart Grid Technology and Equipment, Nanjing 210096, China
[3]State Grid Jiangsu Electric Power Company Ltd., Nantong Electrical Power Supply Company, Nantong 226001, China

Corresponding author: Wei Gu (wgu@seu.edu.cn)

This work was supported in part by the National Natural Science Foundation of China under Grant 51707033, in part by the Jangsu Key Laboratory of Smart Grid Technology and Equipment, and in part by the Scientific Project of the Jiangsu Electric Power Company.

ABSTRACT With the rapid integration of renewables, optimal economic dispatch in active distribution systems faces great challenges because of the randomness and volatility of renewable energy. This paper presents a robust energy management model considering the temporal and spatial correlation of solar energy in active distribution network. The Pearson autocorrelation and cross-correlation coefficients are calculated to verify the necessity of temporal and spatial correlation, respectively, based on historical data in Jiangsu Province, China. Next, correlation constraints are proposed based on the confidence level, which is nonlinear, and can be linearized due to the discrete feature of polyhedral single-interval uncertainty sets. Then, a two-stage min-max-min robust energy management model considering the correlation constraints and the uncertainty of solar energy is proposed. The first stage aims to determine the operating state of capacity banks and on-load tap changers. The second stage optimizes power dispatch in the worst-case scenario. The column-and-constraints algorithm is implemented to obtain an optimal dispatch strategy that minimizes the operating cost under the worst-case scenario. A case study demonstrates the accuracy and efficiency of the proposed model and presents the influence of temporal and spatial correlation.

INDEX TERMS Robust energy management, active distribution systems, temporal correlation, spatial correlation, correlation constraints.

NOMENCLATURE

A. ABBREVIATIONS

PV	Photovoltaics
DG	Diesel generator
CB	Capacitor banks
ESS	Energy storage system
SVC	Static var compensators
OLTC	On-load tap changers
IL	Interruptible load
BFM	Branch flow model
O&M	Operation and maintenance
C&CG	Column-and-constraints generation
SOCR	Second-order cone relaxation

B. FUNCTIONS

C	Total cost
C^{grid}	Price for main grid power
C^{DG}	Price for diesel generator
$C^{\text{CB,O\&M}}$	O&M cost of CB
$C^{\text{OLTC,O\&M}}$	O&M cost of OLTC
$C^{\text{ESS,O\&M}}$	O&M cost of ESS
$C^{\text{L,cut}}$	Penalty cost for load shedding

C. SETS AND INDICES

i,j,k	Index for buses
ij	Index for branches
t	Index for the time period
m	Index for iteration for C&CG algorithm
$u(j),v(j)$	Set of buses whose parent/child is j
$\varphi_{\text{DG,ESS,OLTC,IL}}$	Set of buses connected with DG/ESS/OLTC/IL

The associate editor coordinating the review of this manuscript and approving it for publication was Jenny Mahoney.

D. PARAMETERS

$p^{*}_{1t}, p^{+}_{1t}, p^{-}_{1t}$	Predicted nominal, upper/low deviation power of PV connected with bus 17 in t
$p^{*}_{2t}, p^{+}_{2t}, p^{-}_{2t}$	Predicted nominal, upper/lower deviation power of PV connected with bus 32 in t
r_{ij}, x_{ij}	Resistance/reactance of branch ij
$V_j^{\min}$, $V_j^{\max}$	Lower/upper bound of voltage at bus j
$I_{ij}^{\max}$	Current capacity limit of branch ij
$P_{j,t}^{\mathrm{PV,pre}}$	Predicted nominal power of PV connected to bus j at the time period t
$P_{j,t}^{\mathrm{d}}$, $Q_{j,t}^{\mathrm{d}}$	Active/reactive load for bus j at the time period t
c_1, c_2, c_3	Fuel cost coefficient of DG
$r^{\mathrm{ESS,O\&M}}$	O&M cost coefficient of ESS
$r^{\mathrm{OLTC,O\&M}}$	O&M cost coefficient of OLTC
$r^{\mathrm{IL,cut}}$	Penalty cost coefficient for load shedding
$S_j^{\mathrm{PV/DG/ESS,max}}$	The maximum inverter capacity for bus j connected to PV/DG/ESS
$R_j^{\mathrm{DG,up}}$, $R_j^{\mathrm{DG,down}}$	The limit of ramping up/down rate of DG
$Q_j^{\mathrm{SVC,min}}$, $Q_j^{\mathrm{SVC,max}}$	The minimum/maximum reactive power of SVC connected to bus j
$N_j^{\mathrm{CB,max}}$	The maximum number of CB for bus j
$Q_j^{\mathrm{CB,step}}$	The reactive power of per unit CB
$B_j^{\mathrm{CB,step}}$	The maximum switching number of CB
$P_j^{\mathrm{IL,max}}$	The maximum IL connected to bus j
k_{ij0}	The initial position of OLTC connected to branch ij
$M_{ij}^{\min}$, $M_{ij}^{\max}$	Lower/upper bound of OLTC connected to branchij
$\Delta k_{ij,t}$	Deviation between two taps of OLTC
$E_j^{\mathrm{bat,max}}$	Maximum energy storage of ESS connected to bus j
η^{ch}, η^{dis}	Charge and discharge efficiency of ESS
$P_j^{\mathrm{ch,max}}$,$P_j^{\mathrm{dis,max}}$	The maximum charge/discharge power of ESS connected to bus j at the time period t
N_t	Number of all time periods
Δt	Time interval
ρ	Confidence level
Π_1, Π_2	The uncertainty budget
Ω_1, Ω_2	The temporal correlation change budget
Δ	The spatial correlation change budget

E. VARIABLES

$P_{ij,t}$,$Q_{ij,t}$	Active/reactive power from i to j at the time period t
$I_{ij,t}$	Current from i to j at the time period t
$V_{j,t}$	Voltage for bus j at the time period t
$P_{j,t}^{\mathrm{ch}}$, $P_{j,t}^{\mathrm{dis}}$	Charge/discharge power for bus j at the time period t
$P_{j,t}^{\mathrm{PV/DG/IL}}$	Active power for PV/DG/IL connected to bus j at time period t
$Q_{j,t}^{\mathrm{SVC/PV/CB/DG/ESS}}$	Reactive power for SVC/PV/CB/DG/ESS connected to bus j at time period t
k_{ij}	The actual value of OLTC connected to branch ij
$M_{ij,t}$	The actual tap of OLTC connected to branch ij
$N_{j,t}^{\mathrm{CB}}$	The actual number of CB connected to bus j
$B_{j,t}^{\mathrm{CB}}$	1 for CB in switching state in t, 0 otherwise
p_m	The output power of PV in the m-th iteration
y_m	The variable value of the slave problem in the m-th iteration
ω_m	The objective value of the slave problem in the m-th iteration
$E_{j,t}^{\mathrm{bat}}$	Energy storage for bus j in time period t
μ_t^{+}, μ_t^{-}, α_t^{+}, α_t^{-},	Deviation marker for p_t^{+}, $/p_t^{-}$
ε_t^{d+}, ε_t^{u+}, ε_t^{d-}, ε_t^{u-}	Deviation marker for temporal correlation
η_t^{d+}, η_t^{u+}, η_t^{d-}, η_t^{u-}	Deviation marker for temporal correlation
ϑ_t^{d+}, ϑ_t^{u+}, ϑ_t^{d-}, ϑ_t^{u-}	Deviation marker for spatial correlation

I. INTRODUCTION

With the depletion of nonrenewable energy sources and increasingly serious global environmental problems [1], photovoltaic (PV), as an inexhaustible clean energy, has attracted increasing attention and developed rapidly in recent years [2]. However, optimal economic dispatch in active distribution systems meets significant challenges due to the randomness and volatility characteristics of renewable energy [3]. To ensure stable and economic operation, efficient energy management in consideration of uncertainty has attracted significant attention in current research [4].

Traditional analytical strategies with certainty include stochastic programming (SP) [5] and chance-constrained programming [6]. But the effectiveness of the SP relies on the precise probability distribution of photovoltaic, which is difficult to obtain in practice [7]. Chance-constrained programming is guaranteed to be satisfied with confidence level and the optimal solution may be not accurate [8]. Currently, an important method for solving the energy management problem with uncertainty is robust optimization (RO) [9], [10]. Considering the randomness and volatility of renewables, Felipe Valencia *et al.* [11], [12] developed a scenario-based robust energy management system. Scenarios were generated by means of fuzzy interval models. The fuzzy interval provided a range rather than upper and lower boundaries for uncertainty variables. The proposed model can be effectively solved by the interior-point method. Unlike the scenario-based RO model, a robust framework for active and reactive power management in distribution networks using electric vehicles (EVs) were presented in [13]. The uncertainties variables were modeled using deterministic uncertainty sets. The authors of [14] proposed a two-stage RO model in active distribution systems. The uncertainty set was described by the predictive nominal value and interval derivations. The two-stage robust model was solved by a column-and-constraints generation (C&CG) algorithm.

The aforementioned RO models describe the uncertain variables by the polyhedral single-interval uncertainty (SIU) sets based on the interval and budget parameters. The optimal uncertainty parameter results are located at the boundaries of SIU sets in some time periods. In practice, some extreme scenarios are almost impossible, and the SIU sets are overly conservative. To reduce the conservativeness and enhance the practicality of RO in actual situations, the authors of [15] discussed different approaches to construct the uncertainty sets. An interpartitioned uncertainty set was proposed in [16] that reduces the conservativeness in contrast to the SIU sets. In [17], a union of several basic uncertainty sets was presented based on historical data. The proposed uncertainty sets flexibly captured a compact region of uncertainty in a nonparametric fashion. Chengcheng Shao *et al.* [18] proposed a two-stage security-constrained unit commitment model, in which a flexible uncertainty set was applied to describe the uncertainty of wind power. The authors of [19] proposed a robust energy and reserve scheduling model, and the uncertainty sets were treated as adjustable polyhedral uncertainty sets to reduce the conservativeness.

The abovementioned works have made great contributions to reduce the conservativeness of RO. However, these methods reduce the conservativeness by narrowing the range of SIU sets at a mathematical level. They assume the prediction errors among different PV stations and the various scheduling periods are independent of each other. In fact, the assumption of independence may not be guaranteed considering the continuity of scheduling periods and geographical proximity of PV stations. There is a certain correlation between the PV forecast data at the current period and the historical data, which is called temporal correlation. Meanwhile, there is a certain correlation between multiple PV stations in the same area, which is called spatial correlation. However, most of the existing literature has not considered the temporal and spatial correlation in RO, and they are practical and necessary to reduce the conservativeness [20]. The time correlation of wind power prediction error was pointed out directly in [21] based on Irish wind power data, and a model considering the temporal correlation was proposed to reduce the prediction error. The authors of [22] proposed an active distribution grid management based on robust AC optimal power flow. Wind power and PV uncertainty sets were modeled based on spatial-temporal trajectories, while a convex hull technique was used to define the uncertainty sets. Dynamic uncertainty sets were introduced to model the temporal and spatial correlation in [23]. In [24], a multiband uncertainty set with spatial and temporal correlation constraints was formulated by incorporating weight coefficients into the traditional uncertainty budget. However, accurate information about the number of bands and corresponding weight coefficients was hard to obtain, and the study relied on forecast techniques.

To fill the gaps, a robust energy management model considering the temporal and spatial correlation is proposed to cope with the optimal dispatch scheme in active distribution systems. The main contributions include the following:

1) The necessity of temporal and spatial correlation is verified based on historical data. A novel temporal and spatial correlation constraints model is proposed based on the confidence level. Moreover, a novel linearization approach is proposed that converts the nonlinear the temporal and spatial correlation constraints into linear constraints. An uncertainty set considering temporal and spatial correlation is constructed, which is more practical.
2) A novel robust energy management model considering temporal and spatial correlation is proposed in this paper. The novel robust management model is decomposed into a two-stage mixed-integer linear programming (MILP) problem and solved by the C&CG algorithm. The model decreases conservativeness and then effectively reduces operation cost.

The remainder of this paper is organized as follows: In Section II, the necessity of temporal and spatial correlation is verified based on historical data, and an uncertainty set considering temporal and spatial correlation is introduced. Section III describes the robust energy management model in detail. In Section IV, case studies and simulations are presented. Finally, Section V summarizes the study.

II. FORMULATION OF TEMPORAL AND SPATIAL CORRELATION CONSTRAINTS

It is assumed that the uncertain parameters at each moment are independent in traditional SIU sets [4], [14]. In addition, temporal and spatial correlation are not taken into account, which does not correspond with the practical situation.

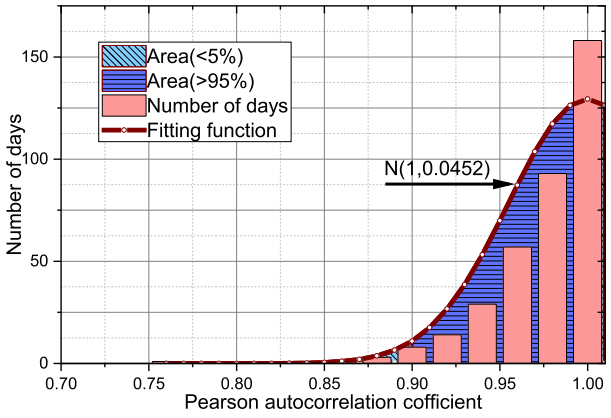

FIGURE 1. Pearson autocorrelation coefficient of output power.

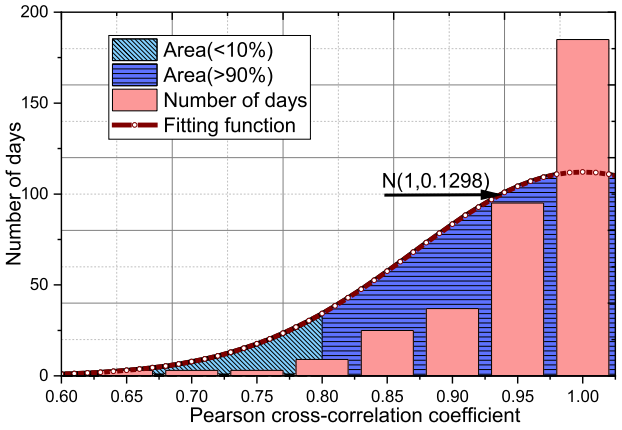

FIGURE 2. Pearson cross-correlation coefficient of output power.

To verify the necessity of temporal and spatial correlation, the Pearson autocorrelation and cross-correlation coefficients are calculated based on historical data from Huai'an City of Jiangsu Province in this section. After that, the temporal and spatial correlation constraints are formulated.

A. THE NECESSITY OF TEMPORAL CORRELATION

To verify the necessity of temporal correlation, the Pearson autocorrelation coefficient, which indicates the correlation of a single sequence at different times, is introduced. The formula for the Pearson autocorrelation coefficient is presented below.

$$C_x(\tau) = \frac{avg\left((x(t) - x^*)\left(x(t+\tau) - x^*\right)\right)}{avg\left((x(t) - x^*)^2\right)} \tag{1}$$

In (1), $avg\,(\cdot)$ is the average function and x^* is the average value of $\boldsymbol{x}$. τ is the time interval (1 h), which is the same as the time interval of forecast data in this study. $C_x(\tau)$ demonstrates the extent to which the historical data affects the current time data. A larger $C_x(\tau)$ means greater impact.

The Pearson autocorrelation coefficient based on the output power of Jixin PV in Huai'an, Jiangsu Province in 2016 is calculated according to equation (2). The results are displayed in Fig. 1.

$$\begin{cases} \boldsymbol{r_0} = [a_1, a_2, \cdots, a_{N_t-1}], \quad \boldsymbol{r_1} = [a_2, a_3, \cdots, a_{N_t}] \\ C(\boldsymbol{r_0}, \boldsymbol{r_1}) = \dfrac{cov(\boldsymbol{r_0}, \boldsymbol{r_1})}{\sigma(\boldsymbol{r_0})\sigma(\boldsymbol{r_1})} \end{cases} \tag{2}$$

In (2), a_t is actual output power of Jixin PV. $\boldsymbol{r_0}$ and $\boldsymbol{r_1}$ are fragments of the Jixin PV output power sequence. $C(\boldsymbol{r_0}, \boldsymbol{r_1})$ and $\mathrm{cov}(\boldsymbol{r_0}, \boldsymbol{r_1})$ are the Pearson autocorrelation coefficient and covariance between $\boldsymbol{r_0}$ and $\boldsymbol{r_1}$, respectively. $\sigma(\boldsymbol{r_0})$ and $\sigma(\boldsymbol{r_1})$ represent the variance of $\boldsymbol{r_0}$ and $\boldsymbol{r_1}$.

The relationship between the Pearson autocorrelation coefficient and the number of days can be fitted to normal distribution N (1, 0.0452) within the given range.

Fig. 1 indicates that the Pearson autocorrelation coefficient of PV in the region is positive. The probability that the Pearson autocorrelation coefficient is more than 0.9 in one year is more than 95%. It is necessary to consider temporal correlation in the robust energy management model.

B. THE NECESSITY OF SPATIAL CORRELATION

To verify the necessity of spatial correlation, the Pearson cross-correlation coefficient that demonstrates the correlation of two sequences at the same moment is introduced. The formula for the Pearson cross-correlation coefficient is presented below.

$$C_y(\tau) = \frac{avg\left((x(t) - x^*)\left(y(t) - y^*\right)\right)}{avg\left(x(t) - x^*\right) avg\left(y(t) - y^*\right)} \tag{3}$$

In (3), x^* and y^* are the average values of sequences $\boldsymbol{x}$, and $\boldsymbol{y}$ separately. $C_y(\tau)$ demonstrates the correlation of two PV power outputs at the same moment. The larger $C_y(\tau)$ means greater correlation.

The Pearson cross-correlation coefficient based on the Jixin PV and ZhaoHui PV output power in Huai'an, Jiangsu Province in 2016 is calculated according to equation (4). The results are depicted as follows.

$$\begin{cases} \boldsymbol{r_0} = [a_{11}, a_{12}, \cdots, a_{1N_t}], \quad \boldsymbol{r_1} = [a_{21}, a_{22}, \cdots, a_{2N_t}] \\ C(\boldsymbol{r_0}, \boldsymbol{r_1}) = \dfrac{cov(\boldsymbol{r_0}, \boldsymbol{r_1})}{\sigma(\boldsymbol{r_0})\sigma(\boldsymbol{r_1})} \end{cases} \tag{4}$$

where a_{1t} and a_{2t} are, respectively, the actual output power of Jixin PV and ZhaoHui PV.

Fig. 2 indicates the Pearson cross-correlation coefficient distribution conforms to N(1, 0.1298) within the given range. The Pearson cross-correlation coefficient of PV in the region is positive. The possibility that the Pearson cross-correlation coefficient is more than 0.8 in one year is 90%. Thus, it is necessary to consider spatial correlation in the robust energy management model.

C. THE TEMPORAL AND SPATIAL CORRELATION CONSTRAINTS

After confirming the necessity of the temporal and spatial correlation, the temporal and spatial correlation constraints are formed as follows.

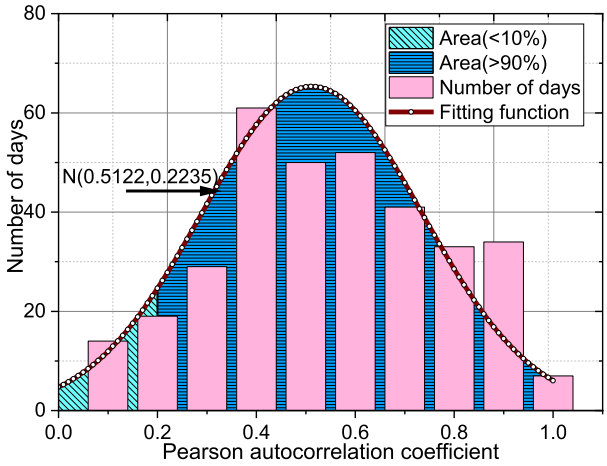

FIGURE 3. Pearson autocorrelation coefficient of prediction derivation.

1) THE TRADITIONAL SIU SET

The traditional SIU set of PV is presented below:

$$\Lambda = \left\{ p \left| \begin{array}{l} p_t = p_t^* + p_t^+ \mu_t^+ - p_t^- \mu_t^- \\ \sum_{t=1}^{N_t} (\mu_t^+ + \mu_t^-) \le \Pi \\ \mu_t^+ + \mu_t^- \le 1, \quad \mu_t^+, \ \mu_t^-, \ \forall t \end{array} \right. \right\} \tag{5}$$

Expression (5) demonstrates that the output power of PV fluctuates within the interval $[p_t^* - p_t^-, p_t^* + p_t^+]$. Π is the uncertainty budget that adjusts the conservativeness level of the robust energy management model. The robust energy management model is a deterministic model if $\Pi = 0$, meaning that the prediction data is absolutely accurate. $\Pi = N_t$ indicates that all the predictions are uncertain over the entire horizon and the model is overly conservative.

2) THE TEMPORAL CORRELATION CONSTRAINT

To analyze the temporal correlation constraint further, the temporal correlation of prediction derivation is introduced to illustrate the extent to which the prediction derivation of the last moment influences the present moment. The Pearson autocorrelation coefficient of the prediction derivation is presented as follows.

$$\begin{cases} e_t = \dfrac{p_t - a_t}{p_t}, \quad \forall t \\ \boldsymbol{s_0} = [e_1, e_2, \cdots, e_{N_t-1}], \quad \boldsymbol{s_1} = [e_2, e_3, \cdots, e_{N_t}] \\ C(\boldsymbol{s_0}, \boldsymbol{s_1}) = \dfrac{cov(\boldsymbol{s_0}, \boldsymbol{s_1})}{\sigma(\boldsymbol{s_0})\sigma(\boldsymbol{s_1})} \end{cases} \tag{6}$$

In (6), p_t and a_t are the predicted and actual values of PV output power. $\boldsymbol{s_0}$ and $\boldsymbol{s_1}$ are fragments of the PV prediction derivation sequence. $C(\boldsymbol{s_0}, \boldsymbol{s_1})$ and $\mathrm{cov}(\boldsymbol{s_0}, \boldsymbol{s_1})$ are the Pearson autocorrelation coefficient and covariance between $\boldsymbol{s_0}$ and $\boldsymbol{s_1}$, respectively. $\sigma(\boldsymbol{s_0})$ and $\sigma(\boldsymbol{s_1})$ represent the variance of $\boldsymbol{s_0}$ and $\boldsymbol{s_1}$. The Pearson autocorrelation coefficient based on the predictive derivation data of Jixin PV in Jiangsu Province in 2016 is displayed in Fig. 3.

Fig. 3 indicates that the probability that the Pearson autocorrelation coefficient for prediction derivation is less than 0.2 is only 10%. Consequently, in order to reduce the size of the uncertainty set further, we remove the low correlation set in the model by introducing the confidence level. Taking Jixin PV as an example, the Pearson autocorrelation coefficient is restricted within the interval (0.2-1) when the confidence level is 0.9 and the coefficient outside this scope can be neglected. Based on the above analysis, the temporal correlation constraint is revealed below.

$$\begin{cases} \boldsymbol{s_0} = [e_1, e_2, \cdots, e_{N_t-1}], \quad \boldsymbol{s_1} = [e_2, e_3, \cdots, e_{N_t}] \\ C(\boldsymbol{s_0}, \boldsymbol{s_1}) \ge \zeta(\rho), \qquad C(\boldsymbol{s_0}, \boldsymbol{s_1}) = \dfrac{cov(\boldsymbol{s_0}, \boldsymbol{s_1})}{\sigma(\boldsymbol{s_0})\sigma(\boldsymbol{s_1})} \end{cases} \tag{7}$$

$\zeta(\rho)$ is the lower bound value related to confidence level ρ, which can be calculated by the fitting function in Fig. 3. The constraint in (7) is a complex nonlinear function, which is difficult to solve and needs to be simplified. Through further analysis, expression (7) can be transformed into a constraint on μ_t^+ and μ_t^- because $\boldsymbol{s_0}$ and $\boldsymbol{s}_1$ are fragments of $\boldsymbol{e}$, and $\boldsymbol{e}$ is composed of μ_t^+ and μ_t^- according to equations (8-9).

$$\left\{ e \left| e_t = \frac{p_t - p_t^*}{p_t^*} = \frac{p_t^+}{p_t^*}\mu_t^+ - \frac{p_t^-}{p_t^*}\mu_t^- = b_1\mu_t^+ - b_2\mu_t^-, \quad \forall t \right. \right\} \tag{8}$$

$$b_1 = \frac{p_t^+}{p_t^*}, \quad b_2 = \frac{p_t^-}{p_t^*} \tag{9}$$

In (9), the coefficients b_1, and b_2 have constant value in this study because the maximum upper/lower derivation are assumed to be 20% of the nominal prediction power. Moreover, the worst-case scenarios occur when the load takes the upper value and the renewables take the lower value [25]. Therefore, it is reasonable to only consider the $\boldsymbol{s}_0^-$ and $\boldsymbol{s}_1^-$ in (7-9) when only the uncertainty of PV is analyzed.

$$\begin{aligned} \boldsymbol{s_0^-} &= b_1 \left[\mu_1^-, \mu_2^-, \cdots, \mu_{N_t-1}^- \right]; \\ \boldsymbol{s_1^-} &= b_1 \left[\mu_2^-, \mu_3^-, \cdots, \mu_{N_t}^- \right] \end{aligned} \tag{10}$$

Based on the above analysis, the original nonlinear constraints describing the temporal constraints in (7) can be rewritten as follows.

$$\begin{cases} \boldsymbol{s_0^-} = b_1[\mu_1^-, \mu_2^-, \cdots, \mu_{N_t-1}^-], \\ \qquad\qquad \boldsymbol{s_1^-} = b_1 \left[\mu_2^-, \mu_3^-, \cdots, \mu_{N_t}^- \right] \\ C(\boldsymbol{s_0^-}, \boldsymbol{s_1^-}) \ge \zeta(\rho), \quad C(\boldsymbol{s_0^-}, \boldsymbol{s_1^-}) = \dfrac{cov(\boldsymbol{s_0^-}, \boldsymbol{s_1^-})}{\sigma(\boldsymbol{s_0^-})\sigma(\boldsymbol{s_1^-})} \end{cases} \tag{11}$$

Expression (11) satisfies two theorems depicted in detail below. For the convenience of description, the temporal change sign ε_t^- is defined in (12) and the sum of ε_t^- is defined as Ω over the whole period.

$$\left\{ \varepsilon^- \left| \varepsilon_t^- = \begin{cases} 0, & \mu_t^- = \mu_{t+1}^- \\ 1, & \mu_t^- \ne \mu_{t+1}^- \end{cases} \right. \right\} \tag{12}$$

Theorem 1: Keep Π constant. The smaller $C(\boldsymbol{s}_0^-, \boldsymbol{s}_1^-)$ is, the larger Ω is.

Proof 1: $\sigma(\boldsymbol{s}_1^-)$ and $\sigma(\boldsymbol{s}_1^-)$ are constant when Π is fixed. $C(\boldsymbol{s}_0^-, \boldsymbol{s}_1^-)$ is determined by $\mathrm{cov}(\boldsymbol{s}_0^1, \boldsymbol{s}_1^-)$ and the formula is presented in the following:

$$cov(\boldsymbol{s_0^-}, \boldsymbol{s_1^-}) = \frac{b_1^2 \sum_{t=1}^{N_t-1} \left(\mu_t^- - s_0^{*-}\right)\left(\mu_{t+1}^- - s_1^{*-}\right)}{N_t - 2} \tag{13}$$

In (13), s_0^{*-} and s_1^{*-} are, respectively, the average values of $\boldsymbol{s_0^-}$ and $\boldsymbol{s_0^-}$ which belong to (0,1). When $\mu_t^- \neq \mu_{t+1}^-$, that is $\varepsilon_t^- = 1$, we have $(\mu_t^- - s_0^{*-})(\mu_{t+1}^- - s_1^{*-}) < 0$. Consequently, the smaller $C(\boldsymbol{s}+_0^-, \boldsymbol{s}+_{\boldsymbol{1}}^-)$ is, the larger Ω is when Π is constant.

Theorem 2: $C(\boldsymbol{s}+_0^-, \boldsymbol{s}+_{\boldsymbol{1}}^-)$ only depends on Π and Ω, which are irrelevant to the specific composition form of $\boldsymbol{s}+_{\boldsymbol{0}}^-$ and $\boldsymbol{s}+_{\boldsymbol{1}}^-$.

Proof 2: (μ_t^-, μ_{t+1}^-) contains four composition forms that are (0,0), (0,1), (1,0) and (1,1). The number of the four forms are defined as k_i. Thus, equation (11) can be rewritten as follows:

$$\begin{aligned} cov(\boldsymbol{s_0^-}, \boldsymbol{s_1^-}) = \frac{b_1^2}{N_t - 2} \{ & k_1 s_0^{*-} s_1^{*-} - k_2 s_0^{*-} \left(1 - s_1^{*-}\right) \\ & - k_3 \left(1 - s_0^{*-}\right) s_1^{*-} + k_4 \left(1 - s_0^{*-}\right)\left(1 - s_1^{*-}\right) \} \end{aligned} \tag{14}$$

Obviously, $\mu_1^- = \mu_{N_t}^-$ when Π is even and $\mu_1^- \neq \mu_{N_t}^-$ when Π is odd. The sum of k_2 and k_3 is Ω. The relationship between k_i, Π, and Ω is depicted in Table 1, which reveals that k_i is constant when Ω and Π are given. $C(\boldsymbol{s}+_0^-, \boldsymbol{s}+_{\boldsymbol{1}}^-)$ is easy to calculate by equation (14), which is irrelevant to the specific form of $\boldsymbol{s}+_0^-$ and $\boldsymbol{s}+_{\boldsymbol{1}}^-$.

Theorem 1 describes a negative correlation between $C(\boldsymbol{s}+_0^-, \boldsymbol{s}+_{\boldsymbol{1}}^-)$ and Ω. Consequently, the lower bound of the temporal correlation can be constrained by limiting the maximum of Ω calculated according to [26].

Theorem 2 reveals that the Pearson autocorrelation coefficients of all scenarios with the given Ω and Π are identical. Therefore, all scenarios existing in expression (5) can be depicted utilizing Ω and Π.

From the analysis above, nonlinear temporal correlation constraints can be transformed into linear constraints related to Ω and Π. The linear constraints are displayed as follows.

$$\Lambda_1 = \left\{ p \left| \begin{array}{l} p_t = p_t^* + p_t^+ \mu_t^+ - p_t^- \mu_t^- \\ \sum_{t=1}^{N_t} (\mu_t^+ + \mu_t^-) \le \Pi \\ \mu_t^+ + \mu_t^- \le 1, \forall t \\ \mu_t^+ - \mu_{t+1}^+ \le \varepsilon_t^{d+}, -\mu_t^+ + \mu_{t+1}^+ \le \varepsilon_t^{u+} \\ \mu_t^- - \mu_{t+1}^- \le \varepsilon_t^{d-}, -\mu_t^- + \mu_{t+1}^- \le \varepsilon_t^{u-} \\ \sum_{t=1}^{N_t} (\varepsilon_t^{d+} + \varepsilon_t^{u+} + \varepsilon_t^{d-} + \varepsilon_t^{u-}) \le \Omega \\ \mu_t^+, \mu_t^-, \varepsilon_t^{d+}, \varepsilon_t^{u+}, \varepsilon_t^{d-}, \varepsilon_t^{u-} \in \{0, 1\} \end{array} \right. \right\} \tag{15}$$

ε_t^{d+}, ε_t^{u+}, ε_t^{d-}, and ε_t^{u-} are introduced for convenience of description. The temporal correlation constraints in (15) are essentially linear constraints related to μ_t^+ and μ_t^-. The uncertainty set considering the temporal constraint in (15) effectively reduces the conservative degree.

TABLE 1. The relationship between k_i and Π, Ω.

k_i	Ω is even	Ω is odd	
		ε_1^-=0	ε_1^-=1
k_1	N_t-1-Π-0.5Ω	N_t-1-Π-0.5Ω	N_t-1-Π-0.5Ω
k_2	Ω/2	(Ω+1)/2	(Ω-1)/2
k_3	Ω/2	(Ω-1)/2	(Ω+1)/2
k_4	(2Π-Ω)/2	(2Π-Ω)/2	(2Π-Ω)/2

Moreover, the temporal constraint is an autocorrelation constraint in essence that is irrelevant to the number of PVs. Consequently, the temporal constraint model is applicable for multiple PVs in real active distribution systems.

3) THE SPATIAL CORRELATION CONSTRAINT

Similar to the Pearson autocorrelation coefficient, the Pearson cross-correlation coefficient based on the prediction derivation of Jixin PV and ZhaoHui PV in Huai'an, Jiangsu Province, in 2016 is displayed as follows.

Fig. 4 shows that the Pearson cross-correlation coefficient of prediction derivation is limited to between (0.3-1) when the confidence level is 0.9, and the coefficient can be neglected beyond that scope. The Pearson cross-correlation coefficient of the prediction derivation is described as follows:

$$\Lambda_2 = \left\{ p \left| \begin{array}{ll} p_{1t} = p_{1t}^* + \beta_t^+ p_{1t}^+ - \beta_t^- p_{1t}^-, & \\ & p_{2t} = p_{2t}^* + \alpha_t^+ p_{2t}^+ - \alpha_t^- p_{2t}^- \\ e_{1t} = \dfrac{p_{1t} - a_{1t}}{p_{1t}}, & e_{2t} = \dfrac{p_{2t} - a_{2t}}{p_{2t}} \\ \boldsymbol{s_0} = [e_{11}, e_{21}, \cdots, e_{N_t 1}], & \\ & \boldsymbol{s_1} = [e_{21}, e_{22}, \cdots, e_{2N_t}] \\ C(\boldsymbol{s_0}, \boldsymbol{s_1}) \ge \zeta(\rho), & \\ & C(\boldsymbol{s_0}, \boldsymbol{s_1}) = \dfrac{cov(\boldsymbol{s_0}, \boldsymbol{s_1})}{\sigma(\boldsymbol{s_0})\sigma(\boldsymbol{s_1})} \end{array} \right. \right\} \tag{16}$$

Expression (16) is nonlinear, which is hard to solve. Similar to temporal correlation constraints, the spatial constraints in (16) can be transformed into the constraints on β_t^- and α_t^- utilizing the processing method in (7-11). The spatial constraints are rewritten as follows.

$$\begin{cases} g_0^- = b_3 \left[\beta_1^-, \beta_2^-, \cdots, \beta_{N_t}^-\right], \\ g_{\boldsymbol{1}}^- = b_4 \left[\alpha_1^-, \alpha_2^-, \cdots, \alpha_{N_t}^-\right] \\ b_3 = \dfrac{p_{1t}^-}{p_{1t}^*}, \quad b_4 = \dfrac{p_{2t}^-}{p_{2t}^*}, \\ C(g_0^-, g_1^-) \ge \zeta(\rho), \quad C(g_0^-, g_1^-) = \dfrac{cov(g_0^-, g_1^-)}{\sigma(g_0^-)\sigma(g_1^-)} \end{cases} \tag{17}$$

Obviously, the constraints in (17) are analogous to the constraints (6-11). Therefore, the spatial change sign ϑ^- is defined below resembling the temporal change sign ε_t^-.

$$\left\{ \vartheta^- \left| \vartheta_t^- = \begin{cases} 0, & \beta_t^- = \alpha_t^- \\ 1, & \beta_t^- \neq \alpha_t^- \end{cases} \right. \right\} \tag{18}$$

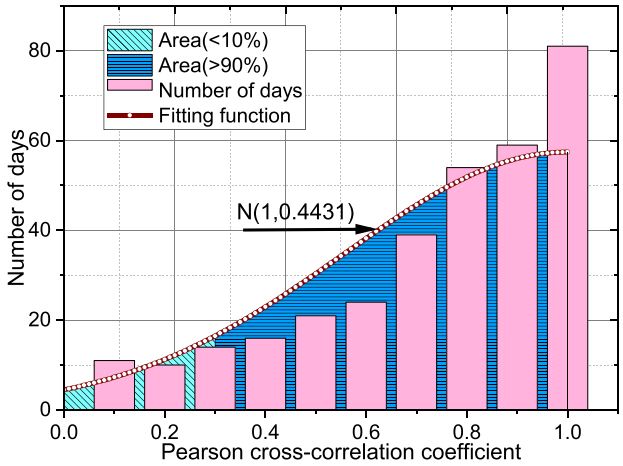

FIGURE 4. Pearson cross-correlation coefficient of the prediction derivation.

The sum of ϑ_t^- is defined as Δ over the whole time period. Similarly, the spatial correlation constraint in (17) can be converted into a linear constraint containing Δ and Π on the basis of the two theorems described above. The linear constraints are depicted as follows.

$$\Lambda_3 = \left\{ p \left| \begin{array}{c} p_{1t} = p_{1t}^* + \beta_t^+ p_{1t}^+ - \beta_t^- p_{1t}^-, \\ p_{2t} = p_{2t}^* + \alpha_t^+ p_{2t}^+ - \alpha_t^- p_{2t}^- \\ \sum_{i=1}^{N_t} (\beta_t^+ + \beta_t^-) \le \Pi_1, \\ \sum_{i=1}^{N_t} (\alpha_t^+ + \alpha_t^-) \le \Pi_2 \\ \beta_t^+ + \beta_t^- \le 1, \quad \alpha_t^+ + \alpha_t^- \le 1, \ \forall t \\ \beta_t^+ - \alpha_t^+ \le \vartheta_t^{d+}, \quad -\beta_t^+ + \alpha_t^+ \le \vartheta_t^{u+} \\ \beta_t^- - \alpha_t^- \le \vartheta_t^{d-}, \quad -\beta_t^- + \alpha_t^- \le \vartheta_t^{u-} \\ \sum_{t=1}^{N_t} (\vartheta_t^{d+} + \vartheta_t^{u+} + \vartheta_t^{d-} + \vartheta_t^{u-}) \le \Delta \\ \beta_t^+, \beta_t^-, \ \alpha_t^+, \ \alpha_t^-, \ \vartheta_t^{d+}, \\ \vartheta_t^{u+}, \ \vartheta_t^{d-}, \ \vartheta_t^{u-} \in \{0, 1\} \end{array} \right. \right\} \tag{19}$$

ϑ_t^{d+}, ϑ_t^{d+}, ϑ_t^{d-}, and ϑ_t^{d-} are introduced for convenience of describing the linear constraints related to β_t^+, β_t^- and α_t^+, α_t^-. Compared to the traditional SIU set, the uncertainty set considering the spatial correlation constraints decreases the conservativeness.

Moreover, the processing method for spatial correlation can extend to multiple PVs. In multiple PV distribution systems, we take one PV as a reference. Then, we construct the spatial correlation constraints between the other PVs and the reference PV based on the above processing method. Consequently, the spatial correlation model is also applicable for multiple PVs.

III. THE ROBUST ENERGY MANAGEMENT MODEL

The robust energy management model aims to minimize the total operating cost in the worst scenario considering the uncertainty of PV and load.

A. THE UNCERTAINTY SET CONSIDERING TEMPORAL AND SPATIAL CORRELATION

The uncertainties cannot be ignored with increasing PV integrated in active distribution systems. Therefore, the optimal energy management model for active distribution systems is a robust energy management model. Based on the above analysis in Section 2, the uncertainty set of PV considering temporal and spatial correlation is composed of (5), (15), and (19). To avoid repetition, the uncertainty set is no longer listed here.

B. THE OBJECTIVE FUNCTION

The total operating cost includes costs from main-grid electricity, diesel generator (DG) fuel, operation and maintenance (O&M), capacitor banks (CB), on-load tap changers (OLTC), energy storage systems (ESS) and the cost of load shedding.

$$\begin{aligned} \min C = {} & C^{\text{grid}} + C^{\text{DG}} + C^{\text{CB,O\& M}} + C^{\text{OLTC,O\& M}} \\ & + C^{\text{ESS,O\& M}} + C^{\text{L,cut}} \end{aligned} \tag{20}$$

$$C^{\text{DG}} = \sum_{j \in \varphi_{\text{DG}}} \sum_{t=1}^{N_t} (c_1 \cdot (P_{j,t}^{\text{DG}})^2 + c_2 \cdot P_{j,t}^{\text{DG}} + c_3) \Delta t \tag{21}$$

$$C^{\text{L,cut}} = \sum_{j \in \varphi_{\text{IL}}} \sum_{t=1}^{N_t} r^{\text{IL,cut}} \cdot P_{j,t}^{\text{IL}} \cdot \Delta t \tag{22}$$

$$C^{\text{OLTC,O\& M}} = \sum_{j \in \varphi_{\text{OLTC}}} \sum_{t=1}^{N_t} r^{\text{OLTC,O\& M}} B_{j,t}^{\text{CB}} \tag{23}$$

$$C^{\text{ESS,O\& M}} = \sum_{j \in \varphi_{\text{OLTC}}} \sum_{t=1}^{N_t} r^{\text{ESS,O\& M}} (P_{j,t}^{\text{ch}} + P_{j,t}^{\text{dis}}) \Delta t \tag{24}$$

Equation (20) represents the total daily operating costs for an active distribution system. Equations (21-24) represent the specific component costs in (20).

C. THE CONSTRAINTS

The constraints in the robust energy management model consist of disflow and operating constraints for all kinds of controllable resources.

1) DISFLOW CONSTRAINTS

$$\left\{ \begin{array}{l} \sum_{i \in u(j)} \left[P_{ij,t} - r_{ij} \left| I_{ij,t} \right|^2 \right] = \sum_{k \in v(j)} P_{jk,t} + P_{j,t} \\ \sum_{i \in u(j)} \left[Q_{ij,t} - x_{ij} \left| I_{ij,t} \right|^2 \right] = \sum_{k \in v(j)} Q_{jk,t} + Q_{j,t} \\ P_{j,t} = P_{j,t}^{\text{d}} + P_{j,t}^{\text{ch}} - P_{j,t}^{\text{dis}} - P_{j,t}^{\text{PV}} - P_{j,t}^{\text{DG}} - P_{j,t}^{\text{IL}} \\ Q_{j,t} = Q_{j,t}^{\text{d}} - Q_{j,t}^{\text{SVC}} - Q_{j,t}^{\text{PV}} - Q_{j,t}^{\text{CB}} - Q_{j,t}^{\text{DG}} - Q_{j,t}^{\text{ESS}} \\ \left| V_{j,t} \right|^2 \cdot k_{ij,t}^2 = \left| V_{i,t} \right|^2 - 2(r_{ij} P_{ij,t} + x_{ij} Q_{ij,t}) \\ \qquad + \left[(r_{ij})^2 + (x_{ij})^2 \right] \left| I_{ij,t} \right|^2 \\ \left| I_{ij,t} \right|^2 = \dfrac{(P_{ij,t})^2 + (Q_{ij,t})^2}{\left| V_{j,t} \right|^2} \end{array} \right. \tag{25}$$

The disflow equation based on the branch flow model (BFM) is nonlinear and difficult to solve. For convenience of calculation, the equivalent transformation ($I_{ij,t} = I_{ij,t}^2$, $V_{j,t} = V_{j,t}^2$), second-order cone relaxation (SOCR) and piecewise linearization are applied to the *disflow* equation [27]. Meanwhile, the accuracy of SOCR was investigated in [28], [29]. To avoid repetition, these transformation methods are not depicted in this paper.

2) OPERATION CONSTRAINTS

The adjustable resources in the active distribution network can be divided into three categories: 1) only participate in active power scheduling, such as interruptible load (IL); 2) only participate in reactive power scheduling, such as CB and static var compensators (SVC); 3) provide both active power and reactive power, such as DG and ESS that deliver a certain amount of reactive power while delivering active power to the distribution network. These constraints are described as follows.

- *Power flow constraint*

$$\begin{cases} V_j^{\min} \le V_{j,t} \le V_j^{\max} \\ 0 \le I_{ij,t} \le I_{ij}^{\max} \end{cases} \tag{26}$$

- *PV operation constraint*
  The active and reactive PV power is limited by the maximum inverter capacity [30] and the constraints are depicted as follows:

$$\begin{cases} P_{j,t}^{\mathrm{PV}} = P_{j,t}^{\mathrm{PV,pre}} \\ \left(P_{j,t}^{\mathrm{PV}}\right)^2 + \left(Q_{j,t}^{\mathrm{PV}}\right)^2 \le \left(S_j^{\mathrm{PV,max}}\right)^2 \end{cases} \tag{27}$$

- *IL operation constraint*

$$0 \le P_{j,t}^{\mathrm{IL}} \le P_j^{\mathrm{IL,max}} \tag{28}$$

- *DG operation constraint*
  Due to the limit of inverter capacity, the active and reactive DG power constraint is revealed as follows.

$$(P_{j,t}^{\mathrm{DG}})^2 + (Q_{j,t}^{\mathrm{DG}})^2 \le (S_j^{\mathrm{DG,max}})^2 \tag{29}$$

  The ramping rate constraint is presented below.

$$\begin{cases} P_{j,t+1}^{\mathrm{DG}} - P_{j,t}^{\mathrm{DG}} \le R_j^{\mathrm{DG,up}} \\ P_{j,t}^{\mathrm{DG}} - P_{j,t+1}^{\mathrm{DG}} \le R_j^{\mathrm{DG,down}} \end{cases} \tag{30}$$

- *SVC operation constraint*

$$Q_j^{\mathrm{SVC,min}} \le Q_{j,t}^{\mathrm{SVC}} \le Q_j^{\mathrm{SVC,max}} \tag{31}$$

- *CB operation constraint*
  The reactive CB power is constrained by the number of CB and the maximum switching number during the scheduling horizon.

$$\begin{cases} Q_{j,t}^{\mathrm{CB}} = N_{j,t}^{\mathrm{CB}} Q_{j,t}^{\mathrm{CB,step}} \\ N_{j,t}^{\mathrm{CB}} \le N_j^{\mathrm{CB,max}} \\ B_{j,t}^{\mathrm{CB}} \in \{0, 1\} \\ \sum_{t=1}^{N_t - 1} B_{j,t}^{\mathrm{CB}} = B^{\mathrm{CB,max}} \\ B_{j,t}^{\mathrm{CB}} Q_{j,t}^{\mathrm{CB,step}} \le \left| Q_{j,t+1}^{\mathrm{CB}} - Q_{j,t}^{\mathrm{CB}} \right| \\ \le B_{j,t}^{\mathrm{CB}} N_j^{\mathrm{CB,max}} Q_{j,t}^{\mathrm{CB,step}} \end{cases} \tag{32}$$

- *OLTC operation constraint*

$$\begin{cases} k_{ij,t} = k_{ij0} + M_{ij,t} \Delta k_{ij,t} \\ M_{ij}^{\min} \le M_{ij,t} \le M_{ij}^{\max} \end{cases} \tag{33}$$

  The OLTC is assumed to have 11 taps with the range of $\pm 5\%$ in this paper.
- *ESS operation constraint*
  Similar to PV, the active and reactive power of ESS is restricted by inverter capacity connected to ESS.

$$\begin{cases} (P_{j,t}^{\mathrm{ch}})^2 + (Q_{j,t}^{\mathrm{ESS}})^2 \le (S_j^{\mathrm{ESS,max}})^2 \\ (P_{j,t}^{\mathrm{dis}})^2 + (Q_{j,t}^{\mathrm{ESS}})^2 \le (S_j^{\mathrm{ESS,max}})^2 \end{cases} \tag{34}$$

To extend life, the ESS battery level should remain within 20%∼90% of the maximum capacity [31].

$$\begin{cases} E_{j,t}^{\mathrm{bat}} = E_{j,t+1}^{\mathrm{bat}} - P_{j,t}^{\mathrm{ch}} \eta^{\mathrm{ch}} \Delta T + P_{j,t}^{\mathrm{dis}} \Delta T / \eta^{\mathrm{dis}} \\ E_{j,N_t}^{\mathrm{bat}} = E_{j,1}^{\mathrm{bat}} - P_{j,N_t}^{\mathrm{ch}} \eta^{\mathrm{ch}} \Delta T + P_{j,N_t}^{\mathrm{dis}} \Delta T / \eta^{\mathrm{dis}} \\ E_j^{\mathrm{bat,max}} \times 20\% \le E_{j,t}^{\mathrm{bat}} \le E_j^{\mathrm{bat,max}} \times 90\% \end{cases} \tag{35}$$

$$0 \le P_{j,t}^{\mathrm{ch}} \le P_j^{\mathrm{ch,max}}, \quad 0 \le P_{j,t}^{\mathrm{dis}} \le P_j^{\mathrm{dis,max}} \tag{36}$$

D. THE MIN-MAX-MIN MODEL

The model presented in (20-36) is a deterministic problem. Nevertheless, some variables, such as the switching positions of OLTC and CB, must adapt to all the scenarios considering the uncertainty of renewable energy. Others can be adjusted with regard to the actual values of the uncertainty set. Therefore, the deterministic model is transformed into a two-stage, ''min-max-min'' robust optimization model in the active distribution system, which can separate the 0-1 variables and continuous variables effectively..

The objective function in (37), as shown at the bottom of the next page, indicates that the outer min model determines the number of CB and the tap of OLTC over the horizon time, which is feasible in any scenario from the uncertainty set. Based on the operating state in the first stage, the inner ''max-min'' model seeks the worst-case scenario and optimizes the operating cost.

IV. SOLUTION METHOD

For the convenience of description, the ''min-max-min'' model is rewritten in matrix form as follows.

$$\min_{\mathbf{x}=\{\mathbf{x_1},\mathbf{x_2}\}} \left\{ \mathbf{c}^{\mathbf{T}}\mathbf{x} + \max_{\mathbf{p}\in\mathbf{P}} \min_{\mathbf{y}\in\Psi\{\mathbf{x},\mathbf{p}\}} \mathbf{d}^{\mathbf{T}}\mathbf{y} \right\} \tag{38a}$$

$$s.t.\ \mathbf{l^x} \le \mathbf{x_1} \le \mathbf{u^x}, \quad \mathbf{x}_2 \in \{0,1\} \tag{38b}$$
$$\mathbf{l^{cx}} \le \mathbf{Ax} \le \mathbf{u^{cx}} \tag{38c}$$
$$\Psi\{\mathrm{x},\mathrm{p}\} = \{\mathbf{l^y} \le \mathbf{y} \le \mathbf{u^y} \tag{38d}$$
$$\mathbf{l^c} \le \mathbf{By} \le \mathbf{u^c} \tag{38e}$$
$$\mathbf{l^c} = \mathbf{l^{cons}} + \mathbf{Ex} + \mathbf{Fp} \tag{38f}$$
$$\mathbf{u^c} = \mathbf{u^{cons}} + \mathbf{Gx} + \mathbf{Hp} \tag{38g}$$
$$\mathbf{y} \in \Omega_{cone}\} \tag{38h}$$

where represents the vector of all operation state variables in the first stage, and $\mathbf{x_1}$, and $\mathbf{x_2}$ represent the vectors of integer and binary variables, respectively. $\mathbf{y}$, and $\mathbf{p}$ represent the vectors of all continuous and uncertainty variables in the second stage, respectively. In addition, $\Psi\{\mathbf{x}, \mathbf{p}\}$ stands for the feasible set under the given $\mathbf{x}$, $\mathbf{p}$. Constraint (38b) presents the lower and upper bound for all variables in the first stage. Constraint (38c) represents linear constraints related to all operating state variables in the first stage. Constraint (38d) denotes the lower and upper bound for all variables in the second stage. Moreover, the linear constraint related to variables in the second stage is presented in (38e). Constraint (38f) indicates that $\mathbf{l^c}$ consists of three components: the constant value $\mathbf{l^{cons}}$, the expression related to $\mathbf{x}$ and the expression related to $\mathbf{p}$. Similarly, constraint (38g) is defined as (38f). In addition, constraint (38h) represents the second-order conic constraint described in (25).

The ''min-max-min'' robust energy management model above is difficult to solve. At present, the Benders decomposition [32] and C&CG algorithm [14], [33] are usually used to solve the model. In this paper, the C&CG algorithm is employed to solve the model because of faster solving speed and fewer iterations compared to Benders decomposition.

A. C&CG ALGORITHM

To cope with the problem, the triple-level ''min-max-min'' model is transformed into a two-stage model consisting of the master and slave problems. The master and slave problems are, respectively, consistent with the first and second stages as described above.

1) SLAVE PROBLEM

The slave problem is a ''max-min'' problem that can be transformed into a single ''max'' problem based on the big-M and dual algorithms. The slave problem is depicted below.

$$\max_{\mathbf{p}\in\mathbf{P}} \min_{\mathbf{y}\in\Psi\{\mathbf{x},\mathbf{p}\}} \mathbf{d^T y} \tag{39a}$$
$$s.t.\ \mathbf{l^y} \le \mathbf{y} \le \mathbf{u^y} \tag{39b}$$
$$\mathbf{l^c} \le \mathbf{Ay} \le \mathbf{u^c} \tag{39c}$$
$$\mathbf{l^c} = \mathbf{l^{cons}} + \mathbf{Ex} + \mathbf{Fp} \tag{39d}$$
$$\mathbf{u^c} = \mathbf{u^{cons}} + \mathbf{Gx} + \mathbf{Hp} \tag{39e}$$
$$\mathbf{y} \in \Omega_{cone} \tag{39f}$$

In (39), $\mathbf{l^{cons}}$, $\mathbf{u^{cons}}$, $\mathbf{Ex}$, and $\mathbf{Gx}$ are constant values when the master problem result $\mathbf{x}$ is given. $\mathbf{F}$ and $\mathbf{H}$ are constant matrices related to $\mathbf{p}$.

- *Dual algorithm*
  The dual algorithm is introduced to convert the ''max-min'' model into a single ''max'' model. The dual algorithm considering the second-order conic constraint is revealed as follows:

$$\max\ (\mathbf{l^c})^T\mathbf{s_l^c} - (\mathbf{u^c})^T\mathbf{s_u^c} + (\mathbf{l^y})^T\mathbf{s_l^y} - (\mathbf{u^y})^T\mathbf{s_u^y} \tag{40a}$$
$$s.t.\ \mathbf{A}^T(\mathbf{s_l^c} - \mathbf{s_u^c}) + \mathbf{s_l^y} - \mathbf{s_u^y} + \mathbf{s_n^y} = \mathbf{d} \tag{40b}$$
$$\mathbf{s_l^c},\quad \mathbf{s_u^c},\ \mathbf{s_l^y},\ \mathbf{s_u^y} \ge 0 \tag{40c}$$
$$\mathbf{s_n^y} \in \Omega_{cone} \tag{40d}$$

$\mathbf{s_l^c}$, $\mathbf{s_u^c}$, $\mathbf{s_l^y}$, and $\mathbf{s_u^y}$ are, respectively, dual variables of $\mathbf{l_c}$, $\mathbf{u_c}$, $\mathbf{l_y}$, and $\mathbf{u_u}$. The expression $\mathbf{s_n^y} \epsilon \Omega_{\mathrm{cone}}$ corresponds with the primal variables in the second-order conic constraint, meaning that $\mathbf{s_n^y}$ have the same format if the variables exist in the $\mathbf{y}$ column vector. Otherwise, $\mathbf{s_n^y}$ should be equal to 0[34].

- *Big_M algorithm*

The objective function in (40a) contains continuous and binary variables simultaneously, such as $\mathbf{l^c s_l^c}$ and $\mathbf{u^c s_u^c}$, which are nonlinear. These bilinear variables can be linearized based on the big_M algorithm.

$$\begin{cases} (\mathbf{l^c})^T\mathbf{s_l^c} = \{(\mathbf{F}(p_{1t}^* + p_{1t}^+\mu_t^+ - p_{1t}^-\mu_t^-))^T + \\ (\mathbf{F}(p_{2t}^* + p_{2t}^+\alpha_t^+ - p_{2t}^-\alpha_t^-))^T\}\mathbf{s_l^c} + (\mathbf{l^{cons}} + \mathbf{Ex})^T\mathbf{s_l^c} \\ (\mathbf{u^c})^T\mathbf{s_u^c} = \{(\mathbf{H}(p_{1t}^* + p_{1t}^+\mu_t^+ - p_{1t}^-\mu_t^-))^T + \\ (\mathbf{H}(p_{2t}^* + p_{2t}^+\alpha_t^+ - p_{2t}^-\alpha_t^-))^T\}\mathbf{s_u^c} + (\mathbf{u^{cons}} + \mathbf{Gx})^T\mathbf{s_u^c} \end{cases} \tag{41}$$

The auxiliary variables are defined as follows:

$$\begin{cases} \gamma_t^+ = (\mu_t^+)^T\mathbf{s_l^c}, & \gamma_t^- = (\mu_t^-)^T\mathbf{s_l^c} \\ \sigma_t^+ = (\mu_t^+)^T\mathbf{s_u^c}, & \sigma_t^- = (\mu_t^-)^T\mathbf{s_u^c} \\ \varpi_t^+ = (\alpha_t^+)^T\mathbf{s_l^c}, & \varpi_t^- = (\alpha_t^-)^T\mathbf{s_l^c} \\ \beta_t^+ = (\alpha_t^+)^T\mathbf{s_u^c}, & \beta_t^- = (\alpha_t^-)^T\mathbf{s_u^c} \end{cases} \tag{42}$$

Therefore, the slave problem model is rewritten as follows. Constraints (43-44) represent the objective function of the slave problem and the dual constraint. Constraints (45-48) indicate the range of auxiliary variables. Constraint (49) represents the uncertainty budget constraint. Constraints (50-51)

$$\min_{\{N_j^{\mathrm{CB}}, B_j^{\mathrm{CB}}, M_{ij}, k_{ij}\}\in x} \{C^{\mathrm{OLTC}} + C^{\mathrm{CB}} + \max_{p\in\mathrm{P}} \min_{\left\{\begin{matrix} P_{ij}, Q_{ij}, V_{ij}, P_j^{\mathrm{DG}}, Q_j^{\mathrm{DG}} \\ P_j^{\mathrm{PV}}, Q_j^{\mathrm{PV}}, P_j^{\mathrm{ch}}, P_j^{\mathrm{dis}}, E_j^{\mathrm{bat}} \end{matrix}\right\}\in y} C^{\mathrm{grid}} + C^{\mathrm{DG}} + C^{\mathrm{ESS,O\&\ M}} + C^{\mathrm{L,cut}}\}$$
$$s.t.\ (5), (15), (19), (25) \text{ to } (36) \tag{37}$$

represent the temporal correlation constraints. Constraint (52) stands for the spatial correlation constraint. Constraint (53) defines all binary variables.

$$\begin{aligned}\max\ & (\mathbf{l^{cons}}+\mathbf{Ex}+\mathbf{Fp^*_{1t}}+\mathbf{Fp^*_{2t}})^T\mathbf{s^c_l}+(\mathbf{l^y})^T\mathbf{s^y_l}\\ & -(\mathbf{u^{cons}}+\mathbf{Gx}+\mathbf{Hp^*_{1t}}+\mathbf{Hp^*_{2t}})^T\mathbf{s^c_u}-(\mathbf{u^y})^T\mathbf{s^y_u}\\ & +\sum_{t=1}^{N_t}(\gamma_t^+p_{1t}^+-\gamma_t^-p_{1t}^-)-\sum_{t=1}^{N_t}(\sigma_t^+p_{1t}^+-\sigma_t^-p_{1t}^-)\\ & +\sum_{t=1}^{N_t}(\varpi_t^+p_{2t}^+-\varpi_t^-p_{2t}^-)-\sum_{t=1}^{N_t}(\beta_t^+p_{2t}^+-\beta_t^-p_{2t}^-)\end{aligned} \tag{43}$$

$$s.t.\ \begin{cases}\mathbf{A}^T(\mathbf{s^c_l}-\mathbf{s^c_u})+\mathbf{s^y_l}-\mathbf{s^y_u}+\mathbf{s^y_n}=\mathbf{d}\\ \mathbf{s^c_l},\mathbf{s^c_u},\mathbf{s^y_l},\mathbf{s^y_u}\geq 0\\ \mathbf{s^y_n}\in\Omega_{cone}\end{cases} \tag{44}$$

$$\begin{cases}-M\mu_t^+\leq\gamma_t^+\leq M\mu_t^+,\ -M\mu_t^-\leq\gamma_t^-\leq M\mu_t^-, & \forall t\\ -s_l^c-M(1-\mu_t^+)\leq\gamma_t^+\leq -s_l^c+M(1-\mu_t^+), & \forall t\\ s_l^c-M(1-\mu_t^-)\leq\gamma_t^-\leq s_l^c+M(1-\mu_t^-), & \forall t\end{cases} \tag{45}$$

$$\begin{cases}-M\mu_t^+\leq\sigma_t^+\leq M\mu_t^+,\ -M\mu_t^-\leq\sigma_t^-\leq M\mu_t^-, & \forall t\\ -s_u^c-M(1-\mu_t^+)\leq\sigma_t^+\leq -s_u^c+M(1-\mu_t^+), & \forall t\\ s_u^c-M(1-\mu_t^-)\leq\sigma_t^-\leq s_u^c+M(1-\mu_t^-), & \forall t\end{cases} \tag{46}$$

$$\begin{cases}-M\alpha_t^+\leq\varpi_t^+\leq M\alpha_t^+,\ -M\alpha_t^-\leq\varpi_t^-\leq M\alpha_t^-, & \forall t\\ -s_l^c-M(1-\alpha_t^+)\leq\varpi_t^+\leq -s_l^c+M(1-\alpha_t^+), & \forall t\\ s_l^c-M(1-\alpha_t^-)\leq\varpi_t^-\leq s_l^c+M(1-\alpha_t^-), & \forall t\end{cases} \tag{47}$$

$$\begin{cases}-M\alpha_t^+\leq\beta_t^+\leq M\alpha_t^+,\ -M\alpha_t^-\leq\beta_t^-\leq M\alpha_t^-, & \forall t\\ -s_u^c-M(1-\alpha_t^+)\leq\beta_t^+\leq -s_u^c+M(1-\alpha_t^+), & \forall t\\ s_u^c-M(1-\alpha_t^-)\leq\beta_t^-\leq s_u^c+M(1-\alpha_t^-), & \forall t\end{cases} \tag{48}$$

$$\sum_{\mathrm{i}=1}^{N_t}(\mu_t^++\mu_t^-)\leq\Pi_1,\quad \sum_{\mathrm{i}=1}^{N_t}(\alpha_t^++\alpha_t^-)\leq\Pi_2 \tag{49}$$

$$\begin{cases}\mu_t^+-\mu_{t+1}^+\leq\varepsilon_t^{d+},\ -\mu_t^++\mu_{t+1}^+\leq\varepsilon_t^{u+}\\ \mu_t^--\mu_{t+1}^-\leq\varepsilon_t^{d-},\ -\mu_t^-+\mu_{t+1}^-\leq\varepsilon_t^{u-}\\ \sum_{t=1}^{N_t}(\varepsilon_t^{d+}+\varepsilon_t^{u+}+\varepsilon_t^{d-}+\varepsilon_t^{u-})\leq\Omega_1\end{cases} \tag{50}$$

$$\begin{cases}\alpha_t^+-\alpha_{t+1}^+\leq\eta_t^{d+},\ -\alpha_t^++\alpha_{t+1}^+\leq\eta_t^{u+}\\ \alpha_t^--\alpha_{t+1}^-\leq\eta_t^{d-},\ -\alpha_t^-+\alpha_{t+1}^-\leq\eta_t^{u-}\\ \sum_{t=1}^{N_t}(\eta_t^{d+}+\eta_t^{u+}+\eta_t^{d-}+\eta_t^{u-})\leq\Omega_2\end{cases} \tag{51}$$

$$\begin{cases}\mu_t^+-\alpha_t^+\leq\vartheta_t^{d+},\ -\mu_t^++\alpha_t^+\leq\vartheta_t^{u+}\\ \mu_t^--\alpha_t^-\leq\vartheta_t^{d-},\ -\mu_t^-+\alpha_t^-\leq\vartheta_t^{u-}\\ \sum_{t=1}^{N_t}(\vartheta_t^{d+}+\vartheta_t^{u+}+\vartheta_t^{d-}+\vartheta_t^{u-})\leq\Delta\end{cases} \tag{52}$$

$$\begin{cases}\mu_t^++\mu_t^-\leq 1,\alpha_t^++\alpha_t^-\leq 1, & \forall t\\ \mu_t^+,\mu_t^-,\varepsilon_t^{d+},\varepsilon_t^{d-},\varepsilon_t^{u+},\varepsilon_t^{u-},\alpha_t^+,\alpha_t^-,\eta_t^{d+},\eta_t^{d-},\\ \eta_t^{u+},\eta_t^{u-},\vartheta_t^{d+},\vartheta_t^{d-},\vartheta_t^{u+},\vartheta_t^{u-}\in\{0,1\}\end{cases} \tag{53}$$

2) MASTER PROBLEM

Assuming that the *k-th* optimal results ($\mathbf{p_k}$, $\mathbf{y_k}$) of the slave problem are acquired, the master problem is depicted below.

$$\min_{\{\mathbf{x_1},\mathbf{x_2}\}\in\mathbf{x},\phi}\ \mathbf{c^T}\mathbf{x}+\phi \tag{54a}$$

$$s.t.\ \mathbf{l^x}\leq\mathbf{x_1}\leq\mathbf{u^x},\quad \mathbf{x_2}\in\{0,1\} \tag{54b}$$

$$\mathbf{l^{cx}}\leq\mathbf{Ax}\leq\mathbf{u^{cx}} \tag{54c}$$

$$\phi\geq\mathbf{d^T}\mathbf{y_k} \tag{54d}$$

$$\mathbf{l^y}\leq\mathbf{y_k}\leq\mathbf{u^y} \tag{54e}$$

$$\mathbf{l^c}\leq\mathbf{By_k}\leq\mathbf{u^c} \tag{54f}$$

$$\mathbf{y_k}\in\Omega_{cone} \tag{54g}$$

The master problem obtains the optimal results $\mathbf{x}$ under the given finite scenarios where $\mathbf{p_k}$ and $\mathbf{y_k}$ are known.

B. SOLVING PROCEDURE

The solving procedure of the two-stage robust energy management model is summarized below:

Initialization: Set a feasible result ($\boldsymbol{x}_0$) to the master problem. The iteration number $m = 1$. Set the lower and upper bound $LB = -\infty$, $UB = +\infty$. Then, set the convergent tolerance ε.

Step 1: Solve the slave problem in (43-53) at $\boldsymbol{x}_0$ and obtain the slave problem results ($\boldsymbol{p_m}$, $\boldsymbol{y_m}$) and the objective ω_m.

Step 2: Solve the master problem at ($\boldsymbol{p_m}$, $\boldsymbol{y_m}$, ω_m) and obtain the master problem results ($\boldsymbol{x}_m$) and the objective φ_m. Meanwhile, the lower bound of the objective function is corrected $LB = \boldsymbol{c}^T\boldsymbol{x}_m + \varphi_m$.

Step 3: Solve the slave problem at ($\boldsymbol{x_m}$) and obtain the slave problem results ($\boldsymbol{p_{m+1}}$, $\boldsymbol{y_{m+1}}$, ω_{m+1}). Meanwhile, the upper bound of the objective function is corrected $UB = \boldsymbol{c}^T\boldsymbol{x}_m + \omega_{m+1}$.

Step 4: If $-\varepsilon < UB - LB < \varepsilon$, the optimization stops and obtains the optimal result. Otherwise, go back to Step 2 and $m = m + 1$.

V. CASE STUDIES

A. BASIC PARAMETERS

The simulation is verified based on the modified IEEE33 presented in Fig. 5. The basic parameters of various controllable resources are listed in Table 2. The prediction data for PV and load are indicated in Fig. 6, and the electricity price refers to [9].

The proposed model is solved in MATLAB R2017a and CPLEX12.8. All numerical simulations are performed on an Intel(R) Core(TM) i7-5500 2.40 GHz, 8G RAM.

TABLE 2. Basic parameters.

Parameters	Value	Parameters	Value	Parameters	Value
$r^{\mathrm{ESS,O\&M}}$(¥/kWh)	0.05	$r^{\mathrm{OLTC,O\&M}}$ (¥/kWh)	0.5	$r^{\mathrm{IL,cut}}$ (¥/kWh)	1.05
$R_i^{\mathrm{DG,up}}$ (kWh)	80	$R_i^{\mathrm{DG,down}}$ (kWh)	80	η^{ch},η^{dis}	0.95
$N_i^{\mathrm{CB,max}}$ (kWh)	4	$B^{\mathrm{CB,max}}$	4	$Q_i^{\mathrm{CB,step}}$ (kvar)	50
$P_i^{\mathrm{ch1,max}}$ (kWh)	200	$P_i^{\mathrm{dis1,max}}$ (kWh)	200	$E_i^{\mathrm{bat1,max}}$ (kWh)	1200
$P_i^{\mathrm{ch2,max}}$ (kWh)	100	$P_i^{\mathrm{dis2,max}}$ (kWh)	100	$E_i^{\mathrm{bat2,max}}$ (kWh)	1000
$S_i^{\mathrm{PV1,max}}$ (kVA)	400	$S_i^{\mathrm{PV2,max}}$ (kVA)	600	$S_i^{\mathrm{ESS,max}}$ (kVA)	400
N_t (h)	24	Δt(h)	1	$\Pi^{\max}$	12

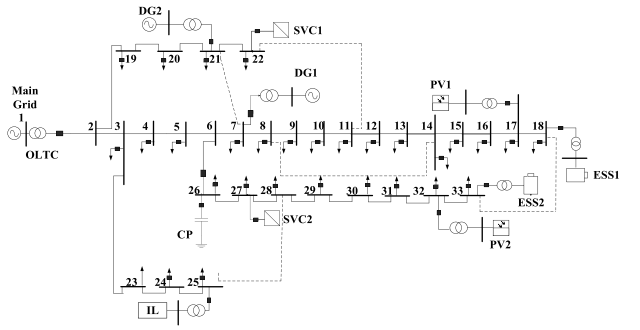

FIGURE 5. The modified IEEE33 distribution system.

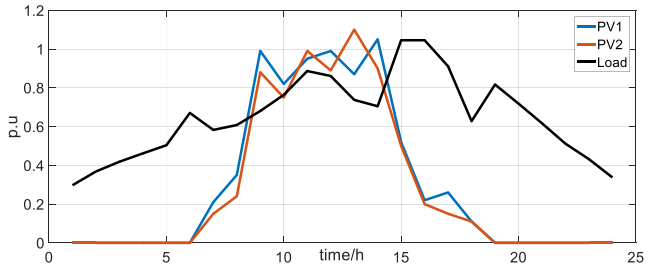

FIGURE 6. The prediction data of load and PV power.

B. ANALYSIS OF THE OPTIMAL RESULTS

To verify the proposed model and solution method, the worst-case scenarios when the Π, Ω, Δ are considered, respectively, are presented in Fig. 7.

Fig. 7(a) presents the optimal result of the traditional robust model [14], in which the uncertainty variables are described by a traditional SIU set. According to Fig. 7(a), we know that the PV output power takes the lower limits when the nominal value is relatively high in the worst-case scenario. This may lead to additional electricity purchasing and increase the operation cost because the PV is less available and the load is relatively high.

Fig. 7(b) shows that the PV output power cannot fluctuate randomly considering the temporal correlation. Due to the limits of fluctuations, the worst-case scenario occurs in consecutive time periods in accordance with weather features. Therefore, the operation cost is lower than the traditional robust model.

Fig. 7(c-d) reveals the optimal results of two PV stations considering temporal and spatial correlation simultaneously. It implies that the worst-case scenario for two PV stations has

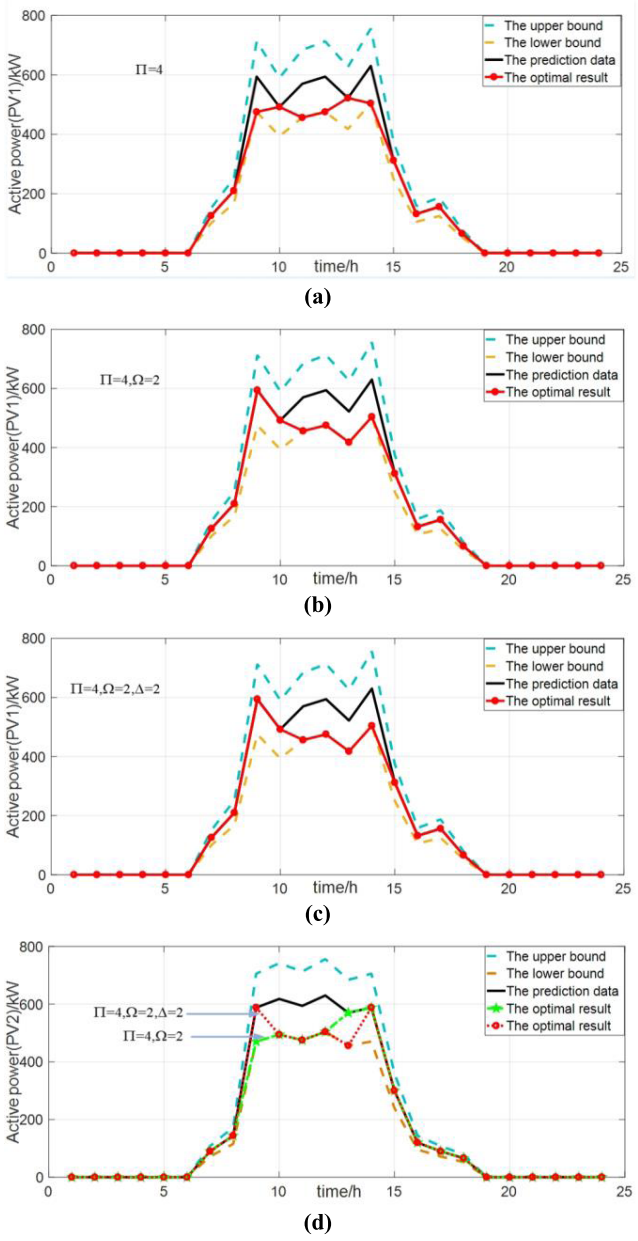

FIGURE 7. The optimal results of the case study.

an obvious correlation because PV output power is mainly determined by climate factors that are less differentiating in the same region.

Meanwhile, the charge and discharge power of ESS in the worst-case scenario when $\Pi = 4$, $\Omega = 2$, and $\Delta = 2$ is displayed in Fig. 8.

From Fig. 8, we observe that the ESS absorbs the active power (7:00-15:00) when PV output increases and the load is relatively low. Then, the stored power discharges in peak load. Consequently, the ESS contributes to reducing the operation cost by shifting the peak load to the valley load. Similarly, the IL can release the load pressure when the load is relatively high.

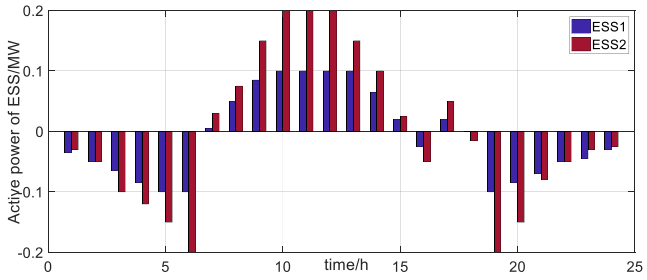

FIGURE 8. Charge and discharge power of ESS.

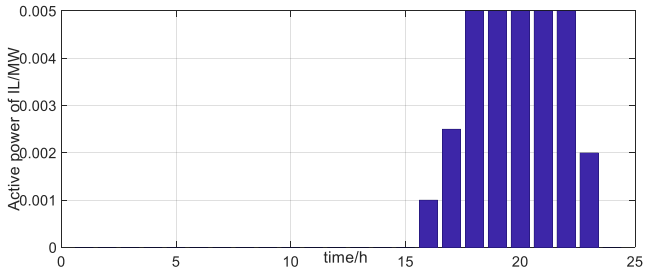

FIGURE 9. Active power of IL.

TABLE 3. The relationship between the pearson correlation coefficient and Π, Ω, and Δ.

Π	Ω	Δ	autocorrelation	cross-correlation
2	2	2	0.4524	0.4525
3	2	2	0.6167	0.6190
4	2	2	0.6974	0.7000
4	2	4	0.6974	0.4000
4	4	2	0.3947	0.7000
4	4	4	0.3947	0.4000

C. COMPARISON OF THE OPTIMIZATION RESULTS AMONG DIFFERENT MODELS

To more effectively analyze the influence of temporal and spatial correlation, the conservative variables Π, Ω and Δ related to the Pearson autocorrelation and cross-correlation coefficients are introduced. The relationships between the Pearson correlation coefficient and Π, Ω, and Δ are presented in Table 3.

Table 3 indicates that there is positive correlation between the Pearson autocorrelation coefficient and Π with the given Ω. The same relationship between the Pearson cross-correlation coefficient and Π is revealed above. To more clearly compare the performance difference between the traditional robust model and the proposed model in this paper, the operation costs of different models are presented in Table 4.

As indicated in Table 4, both the total cost of the traditional robust model and the proposed model are higher than that of deterministic model since the robust model is more conservative. Nevertheless, the proposed model exhibits better performance in the worst-case scenario compared to the traditional robust model with the given Π. With increasing values of Π, the operation cost increases because PV output power takes lower value during more time periods. The comparison highlights that the optimal dispatch scheme of the proposed model is more effective and economical than other models when facing uncertain conditions.

TABLE 4. Operation costs of different models.

Model	Π	Ω	Δ	Total costs (RMB)
Deterministic model	--	--	--	34346.76
Traditional robust model (the SIU set)	2	--	--	34779.31
	3	--	--	34927.80
	4	--	--	35052.75
The proposed model (the proposed uncertainty set)	2	2	2	34658.42
	3	2	2	34775.98
	4	2	2	34860.86

TABLE 5. Operation costs under different Δ and Ω.

Model	Π	Ω	Δ	Total costs (RMB)
Traditional robust model	4	--	--	35052.75
The proposed model	4	2	2	34860.86
	4	2	4	34886.37
	4	4	2	34945.79
	4	4	4	34995.36

To reveal the influence of Δ and Ω, the objective values under different Δ and Ω are depicted in Table 5.

Table 5 compares the total operation cost of the proposed model under different Δ and Ω. The results show the total operating cost increases with increasing value of Ω when Δ is fixed. Similarly, the daily operating cost increases as Δ increases when Ω is fixed. This result implies that there is a negative correlation between the conservativeness and Ω, Δ.

D. SENSITIVITY ANALYSIS OF Π, Ω, AND Δ

To analyze the influence of these conservative variables further, sensitivity analysis under different Π, Ω, and Δ are shown in the following.

1) ANALYSIS OF THE UNCERTAINTY BUDGET Π

Taking the PV station integrated into node 17 in the modified IEEE33 system as an example, with a given Ω, the worst-case scenario under different Π is displayed.

The optimal results between the traditional robust model and the proposed model under different Π are compared in Fig. 10. Fig. 10 (a-d), respectively, illustrate the worst-scenario when $\Pi = 2, 3, 4$, and 5, and $\Omega = 2$. Obviously, with increasing Π value, PV output power takes the lower bound value during more time periods. The comparison demonstrates that the certainty budget enhances the conservative degree and further increases operation cost.

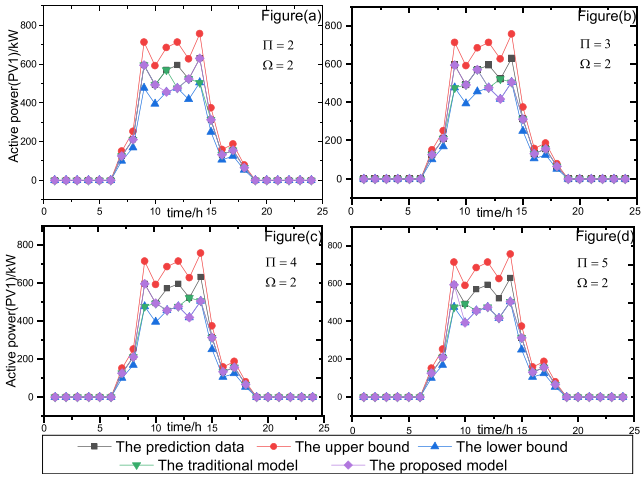

FIGURE 10. Analysis of the worst-case scenarios under different Π.

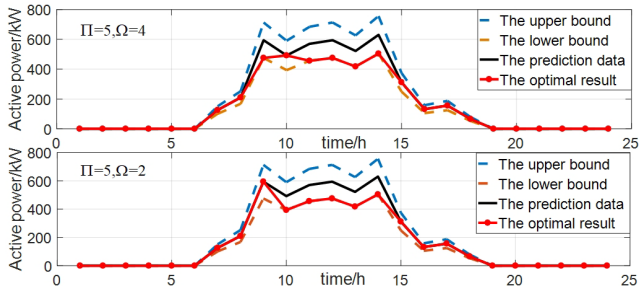

FIGURE 11. Analysis of the worst-case scenarios under different Ω.

2) ANALYSIS OF THE TEMPORAL CORRELATION BUDGET Ω

To reflect the performance difference under different Ω, the optimal results under different Ω when $\Pi = 5$ are depicted in Fig. 11.

Fig. 11 presents the optimal results when $\Pi = 5$, $\Omega = 2$, and 4, respectively. It is apparent that the worst-case scenario in the traditional robust model occurs at the 9:00, and 11:00-14:00 time periods. Nevertheless, considering the temporal correlation, the worst-case scenario occurs at 10:00-14:00 because the output power of PV is determined by climate factors, which do not change randomly. Consequently, the optimal results in the proposed model appear in consecutive time periods due to weather characteristics which are more in line with the actual situation.

3) ANALYSIS OF THE SPATIAL CORRELATION BUDGET Δ

To illustrate the influence of the spatial correlation budget Δ, two PV stations integrated into 17 and 32 nodes, respectively, are taken into consideration. It is assumed that Π is 4, and Ω is 2 in this part. The optimal results under different Δ are described as follows.

Fig. 12 compares the optimal results under different Δ between the traditional and the proposed robust models. The worst-case scenario considering the spatial correlation occurs during similar time periods since the weather is less

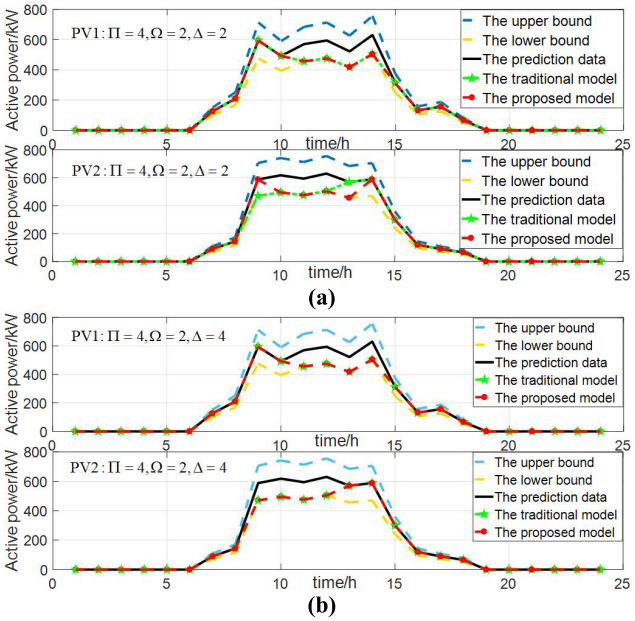

FIGURE 12. Analysis of the worst-case scenarios under different Δ.

differentiating in the same region. Both the traditional and proposed models present the same optimization results in Fig. 12 (b). That is because PV output power is mainly concentrated during the 9:00-14:00 time period. Therefore, it is not necessary to adjust the optimal results with the given parameters $\Pi = 4$, $\Omega = 2$, and $\Delta = 4$. The analysis above indicates the proposed model considering spatial correlation effectively narrows the uncertainty set and decreases the conservativeness.

VI. CONCLUSION

The paper proposes a robust energy management model for active distribution systems simultaneously considering temporal and spatial constraints based on historical data. The uncertainty budget Π, the temporal correlation budget Ω and the spatial correlation budget Δ are introduced as control parameters that influence the conservative degree in the proposed model. The conclusions are presented as follows:

1) The uncertainty set considering the temporal and spatial correlation proposed model narrows the range and reduces the conservativeness degree of the uncertainty set effectively compared to the traditional SIU set.
2) The worst-case scenario occurs during consecutive time periods in the proposed model compared to random fluctuation in the traditional SIU set, which is more consistent with the realistic situation.
3) The proposed model has an economic advantage under the worst-case scenario compared to the traditional robust model.

The proposed model effectively reduces the conservativeness considering the temporal and spatial correlation of PV but fails to consider the correlation between renewable energy and load. Research on the correlation between renewable

energy and load is necessary, and we will leave this topic to the next paper.

REFERENCES

[1] J. F. Zheng, Z. G. Zhou, J. N. Zhao, and J. D. Wang, "Integrated heat and power dispatch truly utilizing thermal inertia of district heating network for wind power integration," *Appl. Energy*, vol. 211, pp. 865–874, Feb. 2018.
[2] W. Gu, J. Wang, S. Lu, Z. Luo, and C. Wu, "Optimal operation for integrated energy system considering thermal inertia of district heating network and buildings," *Appl. Energy*, vol. 199, pp. 234–246, Aug. 2017.
[3] M. Sedighizadeh, M. Esmaili, A. Jamshidi, and M.-H. Ghaderi, "Stochastic multi-objective economic-environmental energy and reserve scheduling of microgrids considering battery energy storage system," *Int. J. Elect. Power*, vol. 106, pp. 1–16, Mar. 2019.
[4] H. Qiu, W. Gu, Y. Xu, and B. Zhao, "Multi-time-scale rolling optimal dispatch for ac/dc hybrid microgrids with day-ahead distributionally robust scheduling," *IEEE Trans. Sustain. Energy*, vol. 10, no. 4, pp. 1653–1663, Oct. 2019.
[5] P. Jirutitijaroen and C. Singh, "Reliability constrained multi-area adequacy planning using stochastic programming with sample-average approximations," *IEEE Trans. Power Syst.*, vol. 23, no. 2, pp. 504–513, May 2008.
[6] M. Mazadi, W. D. Rosehart, O. P. Malik, and J. A. Aguado, "Modified chance-constrained optimization applied to the generation expansion problem," *IEEE Trans. Power Syst.*, vol. 24, no. 3, pp. 1635–1636, Aug. 2009.
[7] Y. Shui, J. Liu, H. Gao, and Q. Gao, "Two-stage distributed robust cooperative dispatch for integrated electricity and natural gas energy systems considering uncertainty of wind power," *Autom. Electr. Power Syst.*, vol. 42, no. 13, pp. 43–50, Jul. 2018.
[8] A. Zhou, M. Yang, Z. Wang, and P. Li, "A linear solution method of generalized robust chance constrained real-time dispatch," *IEEE Trans. Power Syst.*, vol. 33, no. 6, pp. 7313–7316, Nov. 2018.
[9] Y. Shui, H. Gao, J. Wang, Z. Wei, and J. Liu, "A data-driven distributionally robust coordinated dispatch model for integrated power and heating systems considering wind power uncertainties," *Int. J. Elect. Power*, vol. 104, pp. 255–258, Jan. 2019.
[10] I. G. Sardou, M. Zare, and E. Azad-Farsani, "Robust energy management of a microgrid with photovoltaic inverters in VAR compensation mode," *Int. J. Elect. Power*, vol. 98, pp. 118–132, Jun. 2018.
[11] F. Valencia, J. Collado, D. Sáez, and L. G. Marín, "Robust energy management system for a microgrid based on a fuzzy prediction interval model," *IEEE Trans. Smart Grid*, vol. 7, no. 3, pp. 1486–1494, May 2016.
[12] F. Valencia, D. Saez, J. Collado, F. Ávila, A. Marquez, and J. J. Espinosa, "Robust energy management system based on interval fuzzy models," *IEEE Trans. Control Syst. Technol.*, vol. 24, no. 1, pp. 140–157, Jan. 2016.
[13] S. Pirouzi, J. Aghaei, M. A. Latify, G. Yousefi, and G. Mokryani, "A robust optimization approach for active and reactive power management in smart distribution networks using electric vehicles," *IEEE Syst. J.*, vol. 12, no. 3, pp. 2699–2710, Sep. 2018.
[14] H. Gao, J. Liu, and L. Wang, "Robust coordinated optimization of active and reactive power in active distribution systems," *IEEE Trans. Smart Grid*, vol. 9, no. 5, pp. 4436–4447, Sep. 2018.
[15] Y. Dvorkin, M. Lubin, S. Backhaus, and M. Chertkov, "Uncertainty sets for wind power generation," *IEEE Trans. Power Syst.*, vol. 31, no. 4, pp. 3326–3327, Jul. 2016.
[16] H. Qiu, W. Gu, Y. Xu, Z. Wu, S. Zhou, and J. Wang, "Interval-partitioned uncertainty constrained robust dispatch for AC/DC hybrid microgrids with uncontrollable renewable generators," *IEEE Trans. Smart Grid*, vol. 10, no. 4, pp. 4603–4614, Jul. 2019.
[17] C. Ning and F. You, "Data-driven adaptive robust unit commitment under wind power uncertainty: A Bayesian nonparametric approach," *IEEE Trans. Power Syst.*, vol. 34, no. 3, pp. 2409–2418, May 2019.
[18] C. Shao, X. Wang, M. Shahidehpour, X. Wang, and B. Wang, "Security-constrained unit commitment with flexible uncertainty set for variable wind power," *IEEE Trans. Sustain. Energy*, vol. 8, no. 3, pp. 1237–1246, Jul. 2017.
[19] W. Wei, F. Liu, S. Mei, and Y. Hou, "Robust energy and reserve dispatch under variable renewable generation," *IEEE Trans. Smart Grid*, vol. 6, no. 1, pp. 369–380, Jan. 2015.
[20] L. Xie, P. M. S. Carvalho, L. A. F. M. Ferreira, J. Liu, B. H. Krogh, N. Popli, and M. D. Ilic, "Wind integration in power systems: Operational challenges and possible solutions," *Proc. IEEE*, vol. 99, no. 1, pp. 214–232, Jan. 2011.
[21] G. Bel, C. P. Connaughton, M. Toots, and M. M. Bandi, "Grid-scale fluctuations and forecast error in wind power," *New J. Phys.*, vol. 18, no. 2, 2016, Art. no. 023015.
[22] T. Soares, R. J. Bessa, P. Pinson, and H. Morais, "Active distribution grid management based on robust AC optimal power flow," *IEEE Trans. Smart Grid*, vol. 9, no. 6, pp. 6229–6241, Nov. 2018.
[23] A. Lorca and X. Sun, "Adaptive robust optimization with dynamic uncertainty sets for multi-period economic dispatch under significant wind," *IEEE Trans. Power Syst.*, vol. 30, no. 4, pp. 1702–1713, Jul. 2015.
[24] C. Dai, L. Wu, and H. Wu, "A multi-band uncertainty set based robust SCUC with spatial and temporal budget constraints," *IEEE Trans. Power Syst.*, vol. 31, no. 6, pp. 4988–5000, Nov. 2016.
[25] R. Jiang, J. Wang, and Y. Guan, "Robust unit commitment with wind power and pumped storage hydro," *IEEE Trans. Power Syst.*, vol. 27, no. 2, pp. 800–810, May 2012.
[26] A. Hussain, V.-H. Bui, and H.-M. Kim, "Robust optimal operation of AC/DC hybrid microgrids under market price uncertainties," *IEEE Access*, vol. 6, pp. 2654–2667, 2017.
[27] B. Liu, L. Feng, S. Mei, and X. Zhang, "Optimal power flow in active distribution networks with on-load tap changer based on second-order cone programming," *Autom. Electr. Power Syst.*, vol. 39, no. 19, pp. 40–47, Oct. 2015.
[28] L. Gan, N. Li, S. H. Low, and U. Topcu, "Exact convex relaxation of optimal power flow in radial networks," *IEEE Trans. Autom. Control*, vol. 60, no. 1, pp. 72–87, Jan. 2015.
[29] L. Gan and S. H. Low, "Optimal power flow in direct current networks," *IEEE Trans. Power Syst.*, vol. 29, no. 6, pp. 2892–2904, Nov. 2014.
[30] A. Gabash and P. Li, "Active-reactive optimal power flow in distribution networks with embedded generation and battery storage," *IEEE Trans. Power Syst.*, vol. 27, no. 4, pp. 2026–2035, Nov. 2012.
[31] H. Tan, L. Zhang, P. W. Cong, W. Tang, G. Ceng, D. Yang, and X. Li, "Day-ahead reactive power scheduling for distribution network considering coordination of distributed generation with capacitors," *Power Syst. Technol.*, vol. 38, no. 9, pp. 2590–2597, Sep. 2014.
[32] H. Dashti, A. J. Conejo, R. Jiang, and J. Wang, "Weekly two-stage robust generation scheduling for hydrothermal power systems," *IEEE Trans. Power Syst.*, vol. 31, no. 6, pp. 4554–4564, Nov. 2016.
[33] B. Zhao, H. Qiu, R. Qin, X. Zhang, W. Gu, and C. Wang, "Robust optimal dispatch of AC/DC hybrid microgrids considering generation and load uncertainties and energy storage loss," *IEEE Trans. Power Syst.*, vol. 33, no. 6, pp. 5945–5957, Nov. 2018.
[34] *Duality for Conic Optimization*. Accessed: 2018. [Online]. Available: https://docs.mosek.com/8.1/toolbox/pro-def-conic.html

SUYANG ZHOU, photograph and biography not available at the time of publication.

YI ZHAO received the B.S. degree in electrical engineering from Southeast University, Nanjing, China, in 2017, where he is currently pursuing the M.S. degree in electrical engineering.

WEI GU received the B.S. and Ph.D. degrees in electrical engineering from Southeast University, Nanjing, China, in 2001 and 2006, respectively. From 2009 to 2010, he was a Visiting Scholar with the Department of Electrical Engineering, Arizona State University, Tempe, AZ, USA. He is currently a Professor with the School of Electrical Engineering, Southeast University. His research interests include distributed generations and microgrids, active distribution networks, and integrated energy systems.

ZHI WU received the B.S. degree in mathematics and the M.S. degree in electrical engineering from Southeast University, Nanjing, China, in 2009 and 2012, respectively, and the Ph.D. degree from the University of Birmingham, U.K., in 2016. He is currently a Lecturer with Southeast University. His research interests include renewable energy, and planning and optimization techniques.

YUNPENG LI, photograph and biography not available at the time of publication.

ZHONGHAO QIAN, photograph and biography not available at the time of publication.

YU JI, photograph and biography not available at the time of publication.